Supporting Information for "Strong Coupled Magnetic and Electric Ordering in Monolayer of Metal Thio(seleno)phosphates"

Chenqiang Hua (华陈强)[1], Hua Bai (白桦)[1], Yi Zheng (郑毅)[1], Zhu-An Xu (许祝安)[1], Shengyuan A. Yang (杨声远)[2], and Yunhao Lu (陆赟豪)[*1], and Su-Huai Wei (魏苏淮)[3]

[1] *Zhejiang Province Key Laboratory of Quantum Technology and Device, State Key Laboratory of Silicon Materials, Department of Physics, Zhejiang University, Hangzhou 310027, China*
[2] *Research Laboratory for Quantum Materials, Singapore University of Technology and Design, Singapore 487372, Singapore*
[3]*Beijing Computational Science Research Center, Beijing 100193, China*

1. Calculation methods

Our first-principles calculations within density functional theory (DFT) framework adopted the projector-augmented wave (PAW)[1] method in the Vienna ab-initio simulation package[2]. We chose Perdew, Burke, and Ernzerhof (PBE)[3] of generalized gradient approximation to describe the exchange-correlation functional and HSE06 has been used to check the results[4]. At least 20 Å vacuum layer is added to avoid unphysical interaction between periodic images along z direction. Energy cutoff was set to be 500 eV for all the calculations. For the rectangular unit cell (Fig. 2), the $10 \times 6 \times 1$ Γ-centered *k*-point mesh was adopted to optimize the structure with 0.005 eV/Å and 10^{-6} eV convergence criterion for force and energy, respectively. While for self-consistent calculations, the mesh was increased to $15 \times 9 \times 1$ and the energy convergence criterion was set to 10^{-7} eV. For the magnetic phase transition, the effect of spin-orbit coupling (SOC) is negligible, which was not included here.

Phonon spectra were calculated based on a 2 × 2 × 1 supercell by the finite displacement method using the PHONOPY package[5]. The spin polarized PBE plus U method was considered in the magnetic calculations[6]: U_{eff} = 1eV for Mo^{3+} (see Fig. S7). Besides, we also check the U_{eff} values for Cr and W MTPs and finally we find there is little influence on our results. The calculations of transmission were performed within the Atomistix toolkit (ATK) package based on the non-equilibrium Green's function (NEGF) approach[7].

2. Simultaneous transition of magnetic and electric orderings

In the main text, we introduce the simultaneous transition of magnetic and electric orderings. One is the transition between antiferroelectric (AFE)-antiferromagnetic (AFM) phase (**P**=0 & **M**=0) and ferroelectric (FE)-ferromagnetic (FM) phase (**P**=1 & **M**=1), as shown in Fig. 1. In Fig. S1(a), the other one is the transition between AFE-FM phase (**P**=0 & **M**=1) and FE-AFM phase (**P**=1& **M**=0), which is another exotic multiferroic transition for application and fundamental research.

3. Spontaneous polarization with vibronic Jahn-Teller effect

When M_1 is equal to M_2, 2D MTPs will represent the fascinating 2D materials, *e.g.* the antiferromagnetic (AFM) $Fe_2P_2S_6$ and $Mn_2P_2Se_6$. From the charge analysis of the antiferromagnetic (AFM) $Fe_2P_2S_6$ and $Mn_2P_2Se_6$, the total valence state of P_2X_6 anion sublattice is about -4, thus on the cation sides, the common combination of oxidation state of two TM ions shall be +1/+3 and +2/+2. Similar to $Fe_2P_2S_6$ and $Mn_2P_2Se_6$,

fully replacing TMs with V^{2+}, Cr^{2+}no spontaneous polarization appear, even with Cr^{2+}/W^{2+} combination. Considering the reported polarized states in $CuInP_2S_6$ by second-order Jahn-Teller effect[8], we can replace In^{3+} with unoccupied *d* electrons such as Cr^{3+} in CrI_3 and keep +1 oxidation state of group IB TM such as Cu^{1+} in the MTP compounds. In CuCl semiconductor[8], when moving toward the anion triangle, the A_1 mode of static Cu increase in energy leading a larger mixing between *s* of and *d* orbital. Similarly in Cu*M*P_2X_6, when Cu moving from the center of octahedra to the face of S triangle (O_h to C_{3v}), the A_1 mode of Cu will transition to the top one from O_h to C_{3v} and this may also contribute to Jahn-Teller effect. Beyond this, from the coordination point of view, the Cu^+ favors low coordination rather than six except the $CuCl_6$ octahedra in $CuCl_2$ crystal.

4. Phonon spectra

It is already reported that there are stripe electric AFE (s-AFE) and FE phases in $CuCrP_2S_6$[9]. To verify both two phases survive when the thickness is diminished to monolayer (ML), we calculate the phonon spectrum of ML $CuCrP_2S_6$ with high symmetry non-polar structure in Fig. S2. From the phonon dispersion, we find the soft optical mode appear at both the Brillouin zone (BZ) center Γ and boundary M, which correspond to the vertical motion of neighboring Cu ions in same/opposite directions, respectively. In Fig. S4(c) and (d), phonon spectrum of FE and AFE are plotted, and all modes are positive, indicating the dynamical stability. Furthermore, we find the phonon spectrum of other ML Cu*M*P_2X_6 has no apparent imaginary phonon modes in

the BZ whether in FE or AFE configuration (Fig. S3).

5. Discussions of magnetism with electric transition

Under the crystal field of MX_6 octagedra, the *d* orbitals will split into two groups: lower t_{2g} and higher e_g manifolds in Fig. S4. For the superexchange interaction, the exchange virtual gap (Δ_c) between two manifolds is one of the important factor to affect the way of magnetic exchange interactions. For example, the d^3 configuration of nearly 90° geometry, the ferromagnetic exchange energy will highly related to virtual gap: $E_{FM} \propto \frac{1}{\Delta_c}$, since the hopping from site 1 to site 2 of e_g manifold costs energy. Therefore, the energy cost may larger than energy gain from parallel exchange interactions under Hund's rules, and thus result in antiparallel configuration (AFM). Although the lattice structure is much more complicated and there are multiple exchange paths between the local moments at M^{3+} ions, we still can find the reduction of exchange virtual gap can enhance the FM interactions from AFE to FE from the projected band structure (Fig. 3 and Fig. S5) and MLWFs on-site energy of *d* orbitals in Table S1. To verify this gap change, we further check the Cr^{3+} systems and find similar gap increase from FE to AFE (see Table S1). The magnetic difference is originated from the geometric difference of Cu ions. In AFE, Cu ions are striped and anti-parallel aligned, leading to the small displacement of Mo ions. Similarly in FE, compensatory displacement also appear. From Table S2, we can readily see the difference from the bond length of Mo-S and angle of S-Mo-S in different configurations. Although other exchange contributions will also influence the ground magnetic state, the trend from AFE to FE in M^{3+} MTPs are consistent with each other

(see Table 1 in main text).

6. Strain manipulation

As discussed in the main text, only ML $CuMoP_2S_6$ is found to be have simultaneous ordering-ordering transition due to contribution of other exchange interactions. However, applying the strain can change the bonding strength (e.g. overlap of the orbitals) and well manipulate the exchange interaction. For example, in Fig. S8, ~ 2% uniaxial strain of ML $CuMoP_2Se_6$ along x or y can tune the magnetic phase in FE and finally achieve the simultaneous ordering-ordering transition as ML $CuMoP_2S_6$.

7. Barrier from CINEB

Based on these monolayer d^3 Cu based MTPs, intriguing magnetoelectric devices can be fabricated. When in AFE ground state, it has low magnetization (AFM or FM). Then the vertical electric field can tune the AFE to FE and thus enlarge the magnetization (stronger FM). Thus for application, the transition barrier between FE and AFE phases needs be investigated by climbing image nudged elastic band method (CINEB)[10]. From AFE to FE, the highest transition barrier is 89.5 meV/Cu in ML $CuMoP_2Se_6$, even lower than ML $CuMoP_2S_6$. Meanwhile, the activation energy barrier for reversal process is 12.1 meV/Cu in Fig. S6. For other MTPs, without lose generality, we calculate the transition barrier of $CuCrP_2Se_6$ as example. In Fig. S6(b), the CINEB determined barrier is quite close to the ML $CuMoP_2Se_6$ with minimal

difference.

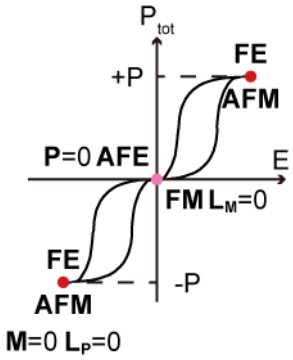

Fig. S1. The FE configuration maintains the AFM state while AFE configuration has FM state. The transition is between AFE-FM phase (P=0 & M=1) and FE-AFM phase (P=1& M=0).

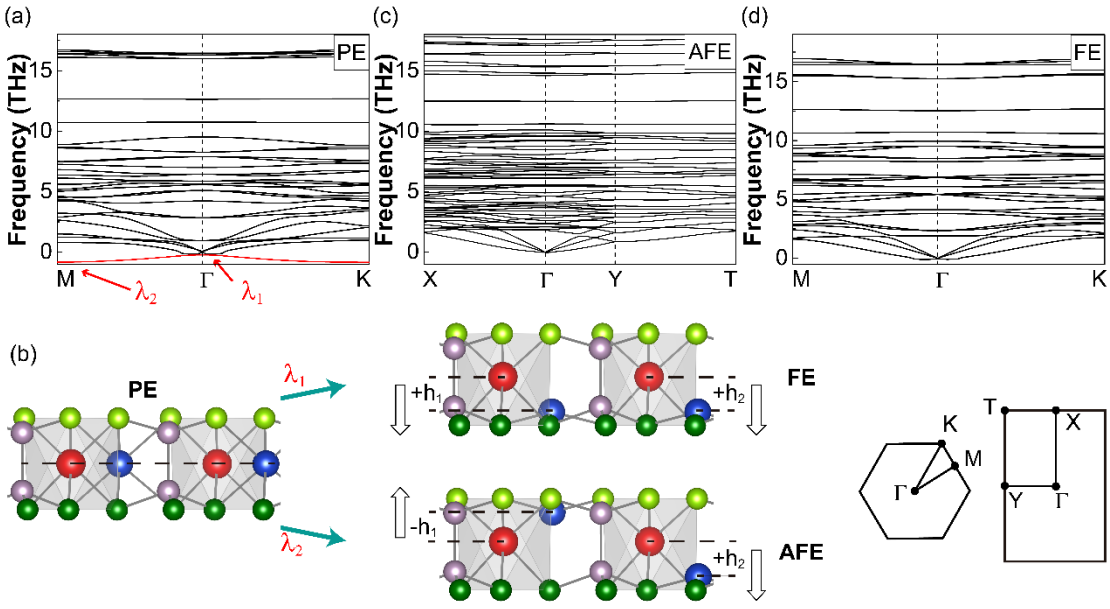

Fig. S2. (a) Phonon spectra of non-polarized monolayer $CuCrP_2S_6$ with soft optical modes. (b) Side views of the different configurations according to soft modes in (a). The height differences between horizontal line and two TM_2 (Cu) are labeled by h_1 and h_2 respectively. (c) – (d) calculated phonon spectrum of AFE and FE $CuCrP_2S_6$ in monolayer limit.

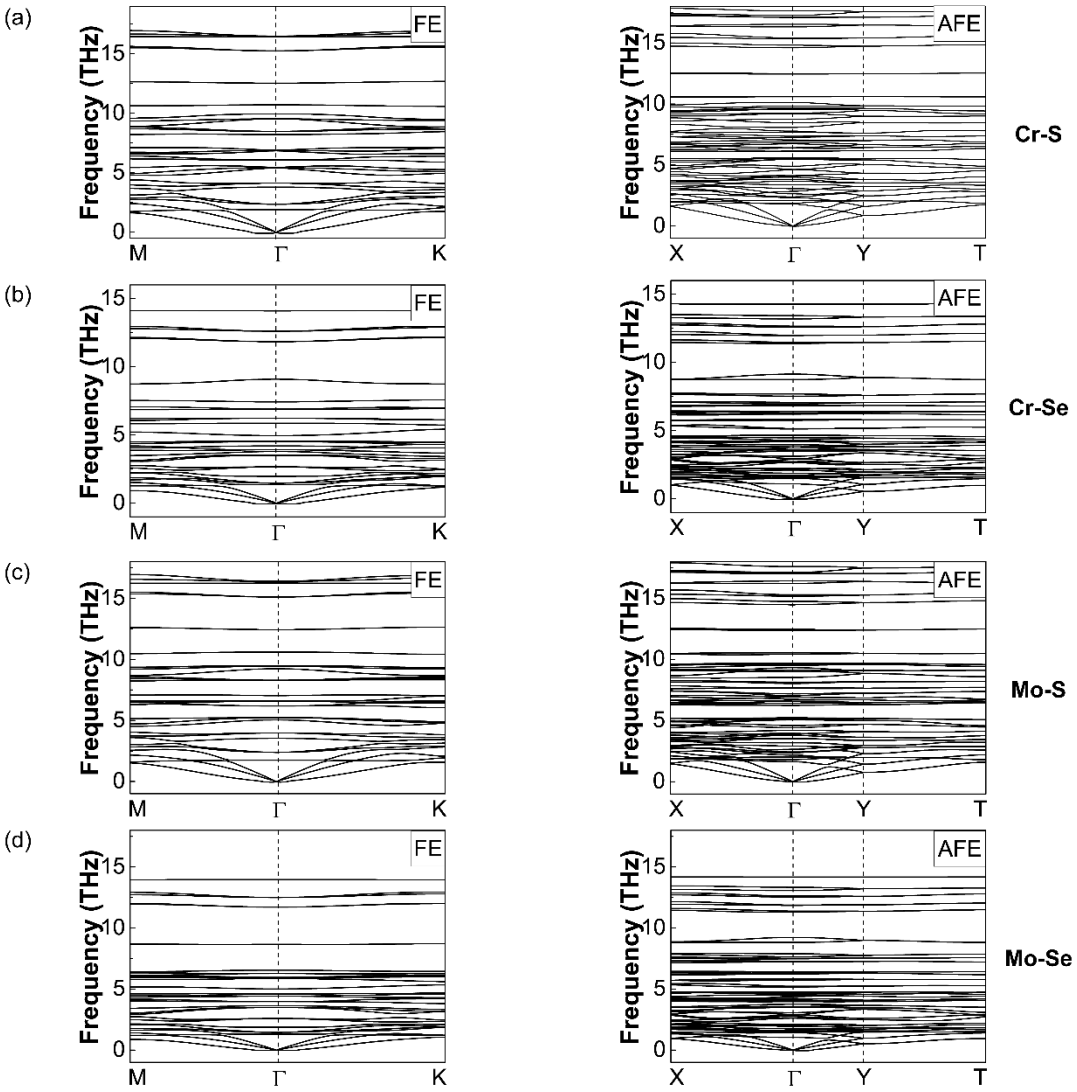

Fig. S3. Phonon spectra of several typical monolayer Cu based MTPs in both AFE and FE configurations. (a) to (d) correspond to Cr-S, Cr-Se, Mo-S and Mo-Se ML systems in both AFE and FE orderings. None of them exhibit obvious imaginary modes in the BZ.

Fig. S4. Under octahedral crystal field, *d* orbitals splitting into t_{2g} and e_g orbitals. Conventionally, the exchange interactions between magnetic ions is highly related to the exchange virtual gap. For example, the hopping from one t_{2g} electron to eg orbitals of another site will cost energy of Δ_c, but follow the Hund's rules, the spin of this electron want to align parallel with spin of t_{2g} electrons. Therefore, the FM or AFM interaction will be the ground state according to the energy competition.

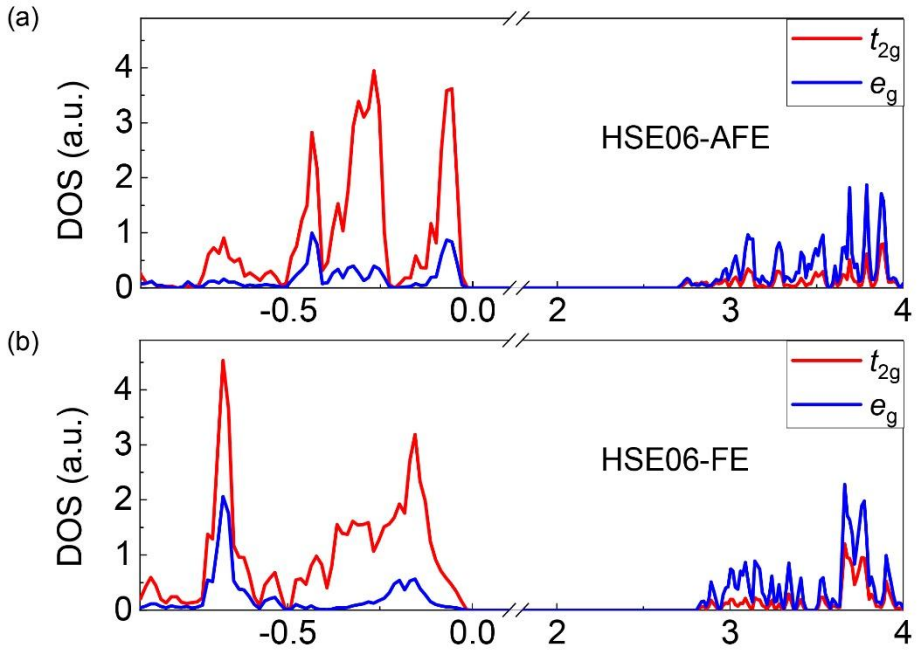

Fig. S5. HSE06 calculated DOS of ML $CuMoP_2S_6$, which is similar to PBE results in the main text Fig. 3. The higher e_g orbitals are also consistent with MLWF energy levels in Table S1.

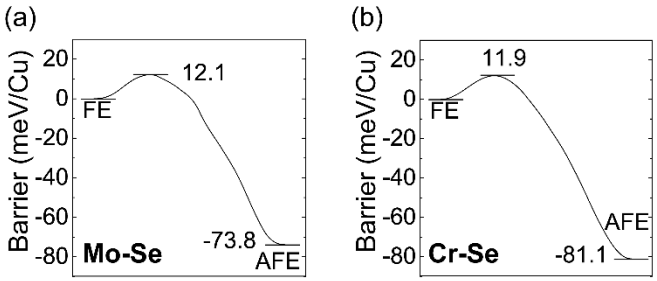

Fig. S6. The calculated barrier between FE and AFE phases of $CuMoP_2Se_6$ by CINEB method. Another plot of calculated barrier of typical system $CuCrP_2Se_6$.

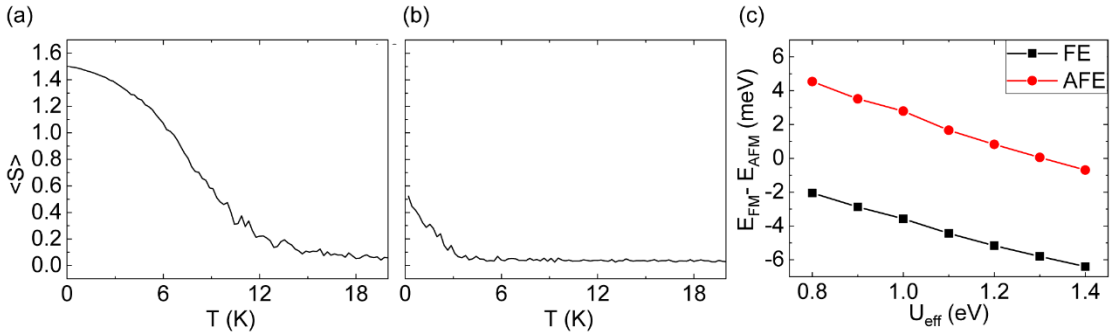

Fig. S7. (a) and (b) Monte Carlo simulation of $CuMoP_2S_6$ FE/AFE monolayer, giving the transition temperature around 15K/5K, defined by the zero averaged spin temperature. (b) Effective Hubbard U_{eff} dependent magnetic phase of $CuMoP_2S_6$ with two electric configurations. Within a large region of U_{eff}, the simultaneous transition of magnetic and electric orderings happen. For the mian results of $CuMoP_2X_6$, the U_{eff} is reasonably set to be 1 eV.

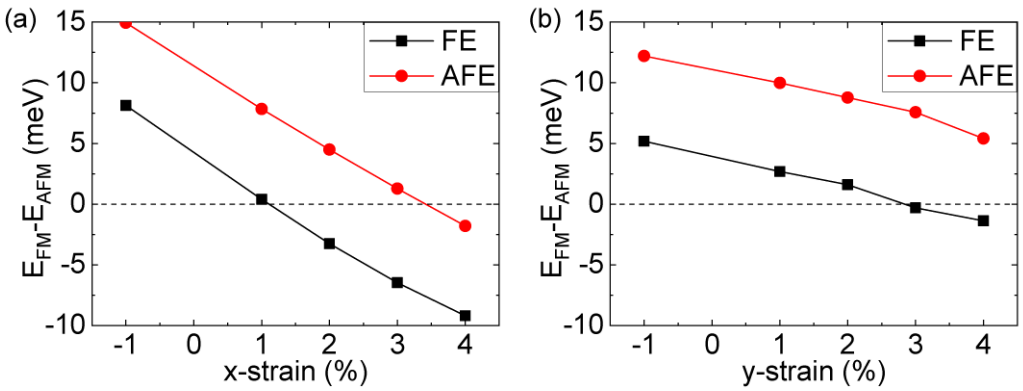

Fig. S8. Uniaxial strain dependent magnetic phase in ML $CuMoP_2Se_6$.

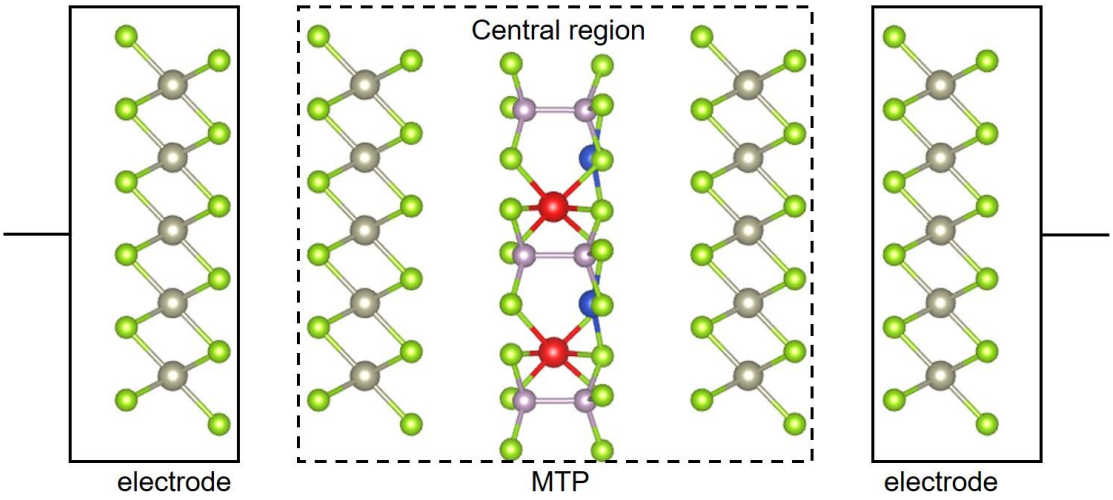

Fig. S9. Schematic figure of MTP based tunneling junction.

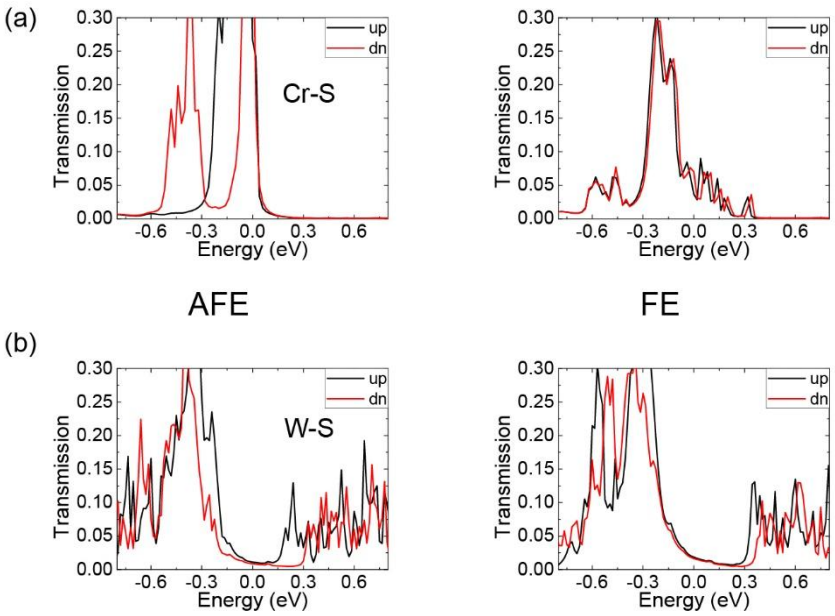

Fig. S10. Calculated transmission spectrum of ML CuCr/WP_2S_6 in both AFE and FE configurations. As expect, the transmission spectrum are nearly degenerated for AFM $CuWP_2S_6$. However, the transmission of FE $CuCrP_2S_6$ doesn't split, which may be originated from the electrode's configuration.

Table S1. MLWFs on-site energy of *d* orbitals: averaged t_{2g} and e_g.

MLWF (eV)	t_{2g}	e_g
Mo-S: FE	0	1.001
Mo-S: AFE	0	1.028
Mo-S: FE-HSE06	0	1.650
Mo-S: AFE-HSE06	0	1.698
Cr-Se: FE	0	1.216
Cr-Se: AFE	0	1.233

Table S2. Bond length and angle in AFE, FE and PE configurations.

Length (Å)	**AFE**	**FE**	**PE**
Mo-$S^{(u)}$	2.537	2.581	2.537
Mo-$S^{(d)}$	2.534	2.496	2.537
Angle (°)	**AFE**	**FE**	**PE**
$S^{(u)}$-Mo-$S^{(u)}$	81.12	78.49	84.64
$S^{(d)}$-Mo-$S^{(d)}$	82.68	85.81	84.64

Table S3. Polarization-dependent effective-exchange-interaction J_1 in Cu$M$$P_2X_6$

d^3 **(meV)**		**Cr-S**	**Mo-S**	**Cr-Se**	**Mo-Se**
J_1	FE	-1.51	-0.25	-1.53	-0.20
	AFE	-0.79	-0.10	-1.24	-0.33

Table S4. Magnetic anisotropy energy (MAE) of $CuMoP_2X_6$, which is defined as E_{001}-E_{100}.

MAE (μeV)	**Mo-S**	**Mo-Se**
FE	637.0	-329.7
AFE	745.0	-301.9

[1] Kresse G and Joubert D 1999 *Phys. Rev. B* **59** 1758–75

[2] Kresse G and Furthmüller J 1996 *Comput. Mater. Sci.* **6** 15–50

[3] Perdew J P, Burke K and Ernzerhof M 1996 *Phys. Rev. Lett.* **77** 3865–8

[4] Tran F and Blaha P 2009 *Phys. Rev. Lett.* **102** 226401

[5] Togo A and Tanaka I 2015 *Scr. Mater.* **108** 1–5

[6] Dudarev S L, Botton G A, Savrasov S Y, Humphreys C J and Sutton A P 1998 *Phys. Rev. B* **57** 1505–9

[7] Brandbyge M, Mozos J-L, Ordejón P, Taylor J and Stokbro K 2002 *Phys. Rev. B* **65** 165401

[8] Wei S-H, Zhang S B and Zunger A 1993 *Phys. Rev. Lett.* **70** 1639–42

[9] Lai Y, Song Z, Wan Y, Xue M, Wang C, Ye Y, Dai L, Zhang Z, Yang W, Du H and Yang J 2019 *Nanoscale* **11** 5163–70

[10] Sheppard D, Xiao P, Chemelewski W, Johnson D D and Henkelman G 2012 *J. Chem. Phys.* **136** 074103